CHEMISTRY OF MATERIALS

Article

pubs.acs.org/cm

Unusual Selectivity of Metal Deposition on Tapered Semiconductor Nanostructures

Nimai Mishra,[†] Jie Lian,[†] Sabyasachi Chakrabortty,[†] Ming Lin,[‡] and Yinthai Chan*[,†,‡]

[†]Department of Chemistry, National University of Singapore, 3 Science Drive 3, Singapore 117543

[‡]Institute for Materials Research & Engineering, A*STAR, 3 Research Link, Singapore 117602

Supporting Information

ABSTRACT: We describe a surfactant-driven method to synthesize highly monodisperse CdSe-seeded CdS nanoheterostructures with conelike, tapered geometries in order to examine the effects of shape on the location-specific deposition of Au under ambient conditions. Although preferential metal deposition at surface defect sites are generally expected, we found suprisingly that Au growth at the side facets of tapered linear and branched structures was significantly suppressed. Further investigation revealed this to be due to a highly efficient electrochemical Ostwald ripening process which was previously thought not to occur in branched nanostructures such as tetrapods. We exploited this phenomenon to fabricate uniform asymmetrically tipped CdSe-seeded CdS tetrapods with conelike arms, where a solitary large Au tip is found on one of the arms while the other three arms bear Ag_2S tips. Importantly, this work presents a synthetic route toward the selective deposition of metals onto branched semiconductor nanostructures whose arms have nearly symmetric reactivity.

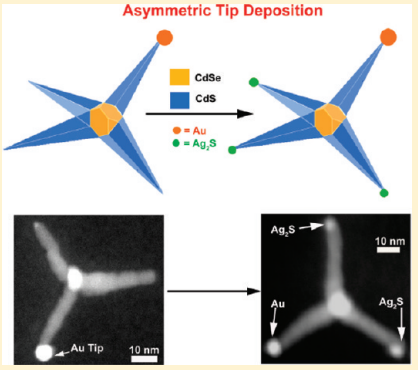

KEYWORDS: *nanorods, tetrapods, metal-semiconductor, Ostwald ripening , gold*

INTRODUCTION

Hybrid metal-semiconductor nanoparticles are promising nanoscale composite materials which potentially exhibit both the physical and chemical characteristics of the individual metal and semiconductor or display unique properties not seen in either component. In the case of anisotropic semiconductor structures such as nanorods, metal nanoparticles grown at the apexes of the rod can serve as electrical connections to enhance charge conductivity.[1] Light-induced separation of charge at the metal-semiconductor interface has also shown utility in photocatalytic processes[2] and in the fabrication of hierarchically complex dumbbell structures.[3] Another opportune application of metal-tipped semiconductor nanorods which exploits the differences in chemical affinity between the surfaces of the metal and semiconductor is in the area of self-assembly, where end-to-end attachment[4] and complex arrangements of Au-tipped nanorods via solvent[5] and ligand-based[6] effects have been demonstrated. In such applications, the topological selectivity of metal deposition and subsequent location on the semiconductor nanostructure is pivotal, and a number of research efforts focusing on the site-selective deposition of metals on nanorods and randomly hyperbranched nanostructures have been reported.[7]

In the case of anisotropic structures such as CdSe-seeded CdS semiconductor nanorods it has been shown that under conditions of UV irradiation, controlled temperature and presence of a suitably passivating ligand, large Au particles can grow selectively at the sulfur-rich facets located at one end of the rod.[8] While the selectivity of the Au deposition can be relatively high (~70% at the S-rich tip[8b]), strict control over multiple parameters and the ensuring of uniform light excitation in scaled-up processes may prove to be fairly challenging. More recently, a facile approach obviating the use of light excitation and requiring the concentration of the Au precursor added as the only parameter tuned was reported, exploiting the inherent differences in reactivity between the facets at the vertices and sides of CdS to achieve site-specific Au deposition.[9] However, determining the optimal Au monomer concentration necessary to minimize nonselective placement of Au throughout the nanorod while allowing for heterogeneous Au nucleation and growth often requires numerous trials, which can be laborious and time-consuming.

Another method for achieving selectivity over the growth of the metal at a particular tip on a semiconductor nanorod may be achieved via an electrochemical Ostwald ripening process reported by Banin et al. in which the smaller metal nanoparticle at one of the tips possesses a higher surface energy and susceptibility to oxidation and slowly dissolves into its individual ions in solution. The electrons left behind by the oxidation of the metal atoms then hop, via surface states, across the semiconductor nanorod surface to the larger metal particle located at the other tip where reduction of the metal ions takes place, thus resulting in an increase in particle size and the eventual formation of a matchstick-like metal-semiconductor

Received: January 15, 2012
Revised: April 27, 2012
Published: May 10, 2012

structure.[10] This reported strategy was, however, demonstrated by the same researchers not to apply to branched structures such as CdSe tetrapods, where the electrochemical Ostwald ripening of Au nanoparticles at the tips of the different arms toward a single dominant arm was not observed.[10] Given the nearly symmetric reactivity of the tips in a tetrapod, varying the concentration of the metal precursor added, which was previously shown to work with nanorods,[9] results in a Poissonian distribution of metal-tipped arms in an ensemble of tetrapods. The controlled and selective deposition of metals onto branched semiconductor structures thus remains a nontrivial and yet important challenge to overcome. We show in this work how such a hurdle may be circumvented via fine structure tuning of the branched nanoparticle.

EXPERIMENTAL SECTION

1. Chemicals. Cadmium acetylacetonate ($Cd(acac)_2$, 99.9%), cadmium oxide (CdO, 99.5%), cadmium acetate ($Cd(ac)_2$, 99.99%) dodecylamine (DDA, 98%), potassium gold(III) chloride ($KAuCl_4$, 99.9%), 1,2-hexadecanediol (HDDO, 90%), 1-hexadecylamine (HDA, 90%), 1-octadecene (ODE, 90%), sulfur (S, reagent grade), selenium (Se, 99.99%), Stearic acid (SA, 98.5%), oleic acid (OA, 90%), myristic acid (MA, 99%), trioctylphosphine oxide (TOPO, 90%), and oleylamine (technical grade, 70%) were purchased from Sigma Aldrich. Trioctylphosphine (TOP, 97%) was purchased from Alfa Aesar. Diisooctylphosphinic acid (DIPA, 90%) was purchased from Fluka. n-octadecylphosphonic acid (ODPA, 97%), trioctylphosphine oxide (TOPO, 99%) and n-hexylphosphonic acid (HPA, 97%) were purchased from Strem. All the chemicals were used as received without further purification. Unless stated otherwise, all the reactions were conducted in oven-dried glassware under nitrogen atmosphere using standard Schlenk techniques.

2. Synthesis of Spherical Zinc Blende CdSe Seeds. Nearly monodispersed zb-CdSe nanocrystals (NCs) were synthesized via a previously reported method.[11] In a 50 mL three-neck round-bottom flask, 0.3 mmol CdO, 0.6 mmol myristic acid and 5 mL of 1-ODE were degassed at 90 °C for about 1 h. The solution was then heated to 250 °C for ∼10−15 min to yield a clear solution, followed by the addition of 12 mL of ODE before cooling to 90 °C to degas for another 1 h. Upon cooling to room temperature, 0.012 g (0.15 mmol) of 100 mesh Se powder (99.999%) was added to the reaction mixture and degassed at 50 °C for ∼20 min. Upon heating to 240 °C under N_2, a color change from colorless to yellow at ∼150 °C and then to orange-red color upon reaching 240 °C were observed, signifying the formation of zb-CdSe nuclei. A degassed mixture of 0.05 mL of oleic acid and 0.5 mL of oleylamine in 2 mL of 1-ODE was subsequently added dropwise to the reaction mixture. As a guideline, the growth time for a ∼4 nm diameter NC was approximately 2 h. As-synthesized zb-CdSe NCs were precipitated out from the growth solution by adding acetone, and were subsequently allowed to undergo two more cycles of redispersion and precipitation in toluene and methanol respectively.

3. Synthesis of Spherical Wurtzite CdSe Seeds. Synthesis of monodispersed w-CdSe NCs proceeded via a previously reported procedure with slight modifications.[12] A bath of 9 g of TOPO (90%), 6 g of HDA, and 0.25 mL of DIPA was degassed at 100 °C for 1.5 h. A precursor solution comprising 317 mg of $Cd(acac)_2$ and 567 mg of HDDO in 6 mL of ODE was degassed at 120 °C for 1.5 h, followed by addition of 4 mL of 1.5 M trioctylphosphine selenide at room temperature. This precursor solution was then rapidly injected into the bath at 360 °C and allowed to cool to 80 °C. The resulting CdSe NCs were subsequently processed by 3 cycles of precipitation in a butanol/methanol mixture and redispersed in toluene for further use.

4. Preparation of Stock Solution of CdSe Seeds. Processed CdSe NCs (zb/w) were dispersed in a minimum amount of toluene and their concentration was determined by measuring their absorbance at 350 nm, whose molar absorptivity is known.[13] The toluene was then removed under vacuum and TOP was added to make up a NC concentration of 100 μM. This mixture will subsequently be referred to as the zb- or w-CdSe stock solution.

5. Synthesis of CdSe-Seeded CdS Heterostructures. Rodlike and tetrapod-like CdSe-seeded CdS heterostructures were synthesized, with slight modifications, via the seeded growth approach.[14] Briefly, 2.65 g of TOPO (99%), 0.05175 g of CdO, and a mixture of ligands were degassed at 150 °C for about 1.5 h in a 50 mL three-neck round-bottom flask. The reaction mixture was then heated to 350 °C under N_2, whereupon the solution turned from reddish brown to colorless. Separately, a mixture of S, TOP, and CdSe seeds was derived by first dissolving a predetermined amount of S in TOP at 50 °C before adding 25 μL of the appropriate CdSe stock solution. Upon reaching the desired injection temperature T °C, an additional amount of TOP was added (1.8 and 0.9 mL in the case of nanorods and tetrapods respectively), and the temperature was allowed to recover to T °C before the mixture of S, TOP, and CdSe was swiftly injected. The temperature was again allowed to recover to T °C and the anisotropic CdS shell (or arms in the case of tetrapods) was grown at this temperature for t minutes. The heating mantle was then removed and the solution was allowed to cool to 80 °C. As-synthesized CdSe-seeded CdS heterostructures were then processed by repeated cycles of precipitation in methanol and redispersion in toluene. A crude approximation of the concentration of the processed CdSe-seeded CdS structures was determined using a previously reported procedure.[15] A summary of the reaction conditions used (values of t and T) for each of the structures described in this work (with the exception of cylinderlike rods) is given in Table S1 in the Supporting Information.

6. Gold Stock Solution Preparation. For the preparation of the Au precursors, 60 mg of $KAuCl_4$ (0.16 mmol) was dissolved in 5 mL of water, yielding a homogeneous clear solution. This will subsequently be referred to as the Au stock solution.

7. Procedure for Gold Growth on CdSe-Seeded CdS Nanoheterostructures. The transfer of $KAuCl_4$ (aqueous solution) from water to toluene was performed following a procedure previously reported by Yang et al.[16] In a 10 mL open top vial, 1 mL of the Au stock solution (which was appropriately diluted when lower Au precursor concentrations was desired) was mixed with 1 mL of a mixture comprising of 280 mg of DDA dissolved in 10 mL ethanol, and allowed to stir for 3 min. To this reaction mixture, 1 mL of a mixture comprising of ∼5 μM CdSe-seeded CdS nanoheterostructures and 6 mg of ODPA in toluene was added and the reaction was allowed to continue for a fixed amount of time, typically ∼1.5 h, and then quenched with MeOH.

8. Procedure for Selective Ag_2S Growth on zb-CdSe/CdS Tapered Tetrapods. In order to initiate growth of Ag_2S at the vertices of zb-CdSe-seeded CdS tetrapods with cone-like arms via cationic exchange between Ag^+ in solution and Cd^{2+} in the nanostructure, transfer of Ag^+ from water to toluene was carried out via a previously reported procedure.[16] Briefly, in a 10 mL open top vial, 1 mL of 0.4 mM aqueous $AgNO_3$ was mixed with 1 mL of a mixture comprising of 280 mg of DDA dissolved in 10 mL of ethanol. After 3 min of continuous stirring, 1 mL of a ∼ 5 μM solution of Au-tipped zb-CdSe-seeded CdS tetrapods with conelike arms in toluene was added and the reaction was allowed to continue for a fixed amount of time, typically ∼30 min, and then quenched with MeOH. The resulting Au- and Ag_2S-tipped tetrapods were then processed by 1−2 cycles of precipitation in methanol and redispersion in toluene before characterization by TEM.

9. Structural Characterization. *Transmission Electron Microscopy.* A JEOL JEM 1220F (100 kV accelerating voltage) or JEOL 2100 (200 kV accelerating voltage) microscope was used to obtain bright-field TEM images of the nanoparticles, respectively. For TEM measurements, a drop of the nanoparticle solution was placed onto a 300 mesh size copper grid covered with a continuous carbon film. Excess solution was removed by an adsorbent paper and the sample was dried at room temperature. The high-resolution TEM images, high-angle annular dark-field scanning-TEM (HAADF-STEM) studies, and detailed elemental composition analysis were carried out on a FEI Titan 80−300 electron microscope operated at 300 KV, which is

dx.doi.org/10.1021/cm300161m | Chem. Mater. 2012, 24, 2040−2046

equipped with an electron beam monochromator, an energy-dispersive X-ray spectroscopy (EDX), and a Gatan electron energy loss spectrometer. The probing electron beam size for the EDX measurement was around 0.3 nm, with a dwell time of ~10 s for each EDX spectrum.

XRD Characterization. X-ray Diffraction (XRD) data was obtained with a diffractometer (Bruker AXS, GADDS) using Cu−K_α radiation (λ = 1.540598 Å) in the range of 20−80°. Samples were prepared on a clean silicon wafer by placing drops of concentrated nanoparticles in toluene on the silicon surface and dried at 80 °C in the oven. This was repeated several times until a thin layer of solid was formed on the silicon substrate.

NMR Characterization. ^{1}H NMR and ^{31}P NMR spectra were recorded on a Bruker ACF 300 and 121 MHz FT-NMR spectrometers and referenced to solvent peaks. Samples were prepared by first completely drying the nanorods and then dispersing them in toluene-d8.

10. Optical Characterization. UV−visible absorption spectra were obtained with an Agilent 8453 UV−visible spectrophotometer. Photoluminescence (PL) spectra were collected with a Shimadzu RF-5301PC Spectrofluorophotometer. Care was taken to ensure that the concentrations of the core and core-seeded nanostructures were sufficiently dilute to avoid contributions from reabsorption or energy transfer.

RESULTS AND DISCUSSION

Given that the mechanism for electrochemical Ostwald ripening of metal nanoparticles on semiconductor nanostructures takes place via the hopping of electrons across surface states, we hypothesized that tapered, conical structures should exhibit enhanced electrochemical Ostwald ripening processes due to the presence of more surface atoms than those of their cylindrical counterparts. In order to test this hypothesis, we developed synthetic procedures to fabricate tapered, conelike analogues of known linear and branched cylinderlike semiconductor nanostructures. Figure 1 summarizes our efforts to produce monodispersed CdSe-seeded CdS rods and tetrapods in accordance with our comparison motif described above. The seeded growth approach of Manna et al.[14,17] with wurtzite CdSe (w-CdSe) and zinc blende CdSe (zb-CdSe) as seeds was used (see the Supporting Information, Table S1), with a key difference that a mixture of n-hexylphosphonic acid (HPA) and oleic acid (OA) was used as surfactants as opposed to n-octadecylphosphonic acid (ODPA) and HPA. Previous reports have suggested that ODPA binds strongly to the (100) side facets of CdS while HPA binds less strongly to the (002) and (00$\bar{2}$) end facets of CdS, resulting in unidirectional growth along the axis of the rod.[15,18] Replacing ODPA with oleic acid and use of w-CdSe cores results in cone-like rods, as shown in Figure 1a. This unusual formation of a cone-like structure may be rationalized by the likely weaker binding of oleic acid to the (100) facets relative to that of ODPA (and to a lesser extent HPA), resulting in extension at the sides of the rod concurrent with growth along its axis. Such a mechanism would be expected to lead to conelike structures with a base much wider than the diameter of the cylindrical-like rods, which is exactly what we found upon comparing the dimensions of the rods in both cases. Employing zb-CdSe seeds in the presence of OA and HPA yielded tetrapods with cone-like arms, as seen in Figure 1b, consistent with the observations obtained with the rods. It is noteworthy that extremely high tetrapod yields of ~85−90% without purification were obtained with the use of HPA and OA. It may be inferred that OA stabilizes the zinc blende phase of CdSe even at elevated temperatures that would typically convert zb- to w-CdSe, consistent with previous

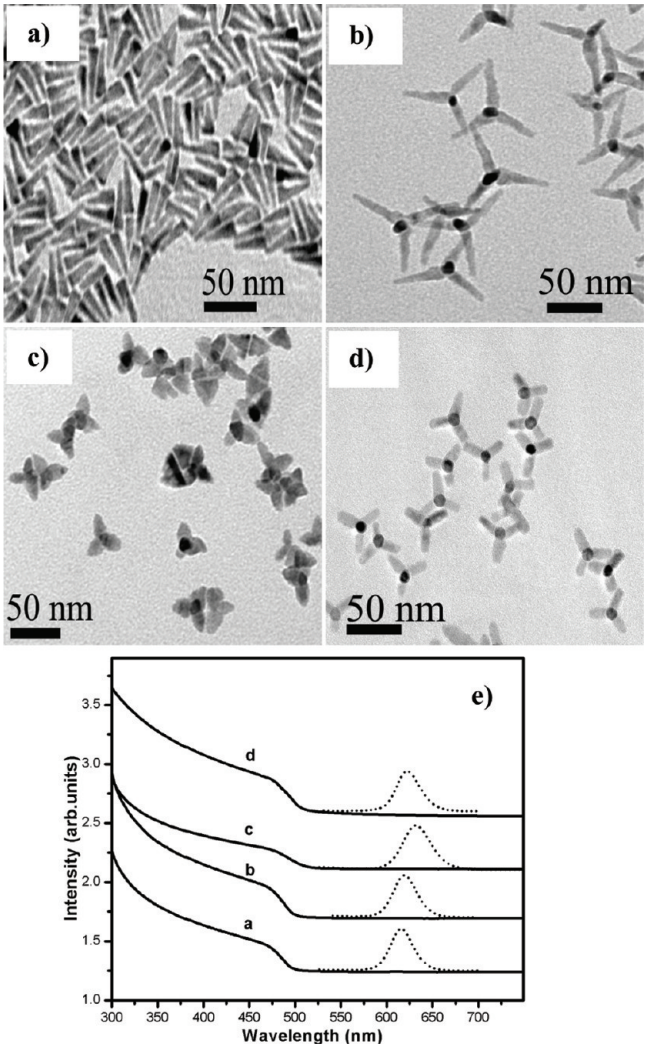

Figure 1. Typical TEM images of various CdSe-seeded CdS nanostructures synthesized using: (a) ~2.9 nm diameter w-CdSe cores, HPA/OA; (b) ~3 nm diameter zb-CdSe cores, HPA/OA; (c) ~3 nm diameter zb-CdSe cores, OA/SA; (d) ~3 nm diameter zb-CdSe cores, HPA/ODPA. (e) Absorption (solid line) and PL (dotted line) spectra of toluene solutions of the different heterostructures shown in a−d.

findings by Mahler et al. for core−shell zb-CdSe/CdS.[19] A reciprocal effect where w-CdSe is converted to zb-CdSe is not seen in mixtures of w-CdSe cores and oleic acid, however, as evident in the high yield (~80%) of unbranched cone-like rods as shown in Figure 1a. When HPA is replaced by another carboxylic acid, stearic acid (SA), the combination of OA and SA leads to fairly monodisperse tetrapods with very wide cone-like arms, as depicted in Figure 1c, further corroborating the cone-like growth mechanism proposed above. For comparison purposes, we also synthesized conventional CdSe-seeded CdS tetrapods with cylinderlike arms using HPA/ODPA as surfactants, as illustrated in Figure 1d. The optical spectra corresponding to the various structures 1a−d are given in Figure 1e, and a redshift in the emission from cone-like rods to tetrapods with conelike arms is readily seen. An additional redshift in the emission may be seen in tetrapods with cylinderlike arms, whereas the furthest redshift occurs in tetrapods with very wide cone-like arms. These observations are consistent with the fact that the extent in which the electron

dx.doi.org/10.1021/cm300161m | *Chem. Mater.* 2012, 24, 2040−2046

wave function in the CdSe core delocalizes out into each CdS arm is dependent on the width of the base of the arms (rods may be taken to effectively have only one arm).

To qualify differences in facet distribution along the sides of the tapered and nontapered structures, we performed HRTEM analyses of randomly chosen tetrapods. For tetrapods, one arm is always positioned perpendicular to the image plane, allowing for characterization of its facets from the viewpoint of its growth axis. In the case of tetrapods from Figure 1d, a well-defined hexagonal tip structure allowing determination of its six (010), (100), (1$\bar{1}$0), (0$\bar{1}$0), ($\bar{1}$00), and ($\bar{1}$10) facets (see the Supporting Information, Figure S3), was apparent, as shown in Figure 2a. A side view analysis of the tetrapod arm, as depicted

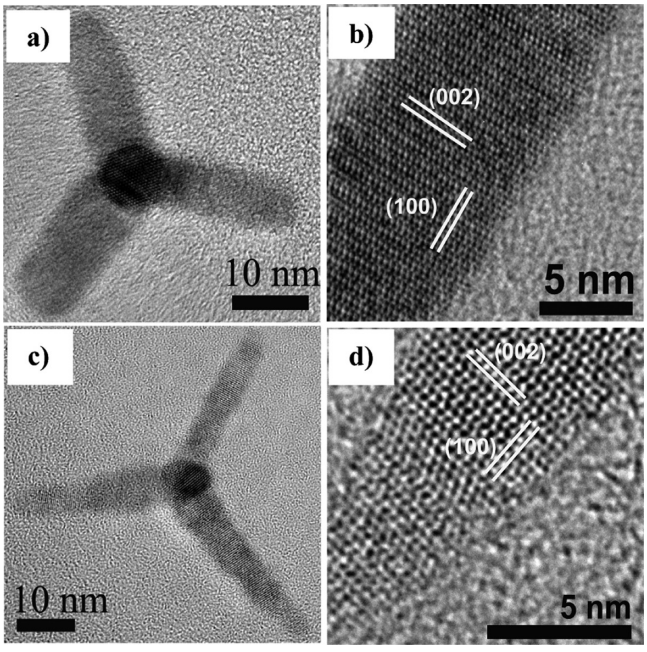

Figure 2. HRTEM images of zb-CdSe-seeded CdS tetrapods with (a) cylindrical- and (c) conelike arms. Imaging along the axis of the arm reveals a well-defined hexagonal tip in a and a distorted hexagon in c. Corresponding magnified views of the arms showed that the side facets are (b) parallel to and (d) deviated from the [100] zone axis, respectively.

in Figure 2(b), revealed the (100) and (002) facets along the length and vertex of the arm respectively. On the other hand, tetrapods from Figure 1b featured a small tip resembling a distorted hexagon atop the conical structure of the arm when viewed along its growth axis and an unambiguous determination of its six facets was extremely difficult, as apparent from Figure 2c. A similar observation was made on tetrapods from Figure 1c (see the Supporting Information, Figure S6). Imaging of the arms lying approximately parallel to the plane of the substrate for these tetrapods, as illustrated in Figure 2d, showed the presence of the (002) facet at the vertex of the arm but with a side facet that is significantly deviated from the [100] zone axis. In contrast with metal nanoparticle surfaces where atomic modeling and direct imaging by HRTEM often reveals a steplike and periodic nature of facets angularly displaced from the growth axis,[20] vicinal surfaces of semiconductors are unlikely to comprise of uniform terraces due to frequent surface reconstruction.[21] The sides of the conelike arms may thus be thought of as a stack of distorted or partially truncated hexagons leading up to the vertex, each layer smaller than the previous as dictated by the conical geometry. It may be inferred that given the nonuniform terrace-like surface morphology of the tapered structure and its subsequent exposure of more surface area, it is likely that the tetrapods with cone-like arms would generally possess a higher number of unpassivated surface atoms relative to those of cylinderlike arms. Indeed, the fluorescence quantum yield (QY) of the cone-like tetrapods (~3 nm CdSe core, ~27 nm CdS arm length) is generally much lower than their cylinderlike (~3 nm CdSe core, ~22 nm arm length) counterparts, with measured QY values of ~11% and ~36%, respectively, further supporting the supposition above and our overall rationale for fabricating tapered structures.

Gold deposition on the various semiconductor nanostructures proceeded via a previously described procedure,[16] with the concentration of the Au precursor as the only parameter varied. Figure 3 is a composite TEM image depicting the

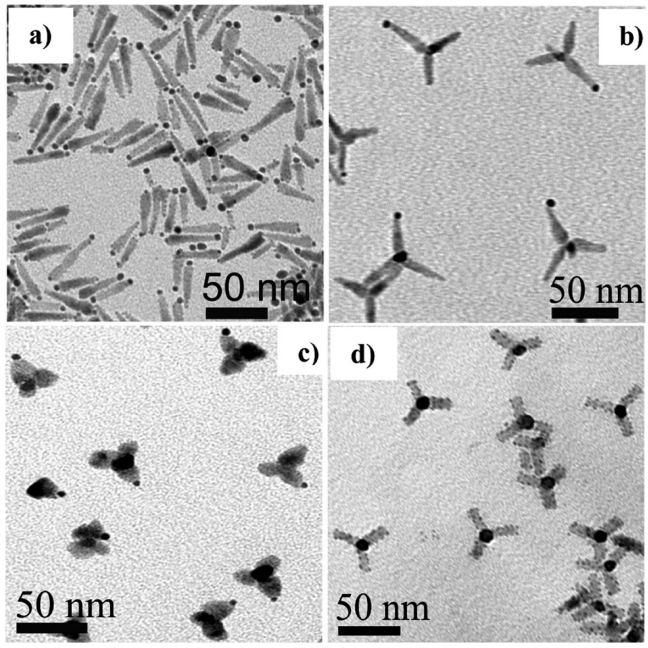

Figure 3. TEM images of structures from Figure 1 exposed to high concentrations of Au precursor. All of the reactions were done at room temperature for a fixed reaction time of 1.5 h.

various Au-decorated surface morphologies obtained for the different anisotropic semiconductor nanostructures upon exposure to relatively high concentrations of Au precursor. Unlike Au deposition on CdSe nanostructures in the presence of dodecylammonium bromide,[7a] exposure to relatively low concentrations of dodecylamine (DDA) within the ~1.5 h reaction time did not result in any discernible etching of the tetrapod arms. While previous reports have shown that Au deposits at the sides and tips of cylinderlike rods at relatively high Au monomer concentrations[7b,9] the cone-like rods showed a marked selectivity for Au growth at the tips even at Au precursor concentrations high enough to observe homogeneous nucleation and growth of isolated Au particles, as shown in Figure 3a. Despite the large excess of Au precursor added, only a small number of minute Au clusters may be seen along the sides of some of the rods, while the Au particles at the tip location were much larger with a diameter of ~6–10 nm. Interestingly, the affinity for tip growth at the sharper end of

dx.doi.org/10.1021/cm300161m | *Chem. Mater.* 2012, 24, 2040–2046

the rod seemingly diminished at high Au precursor concentrations, with a significant number of rods having either a sole or larger Au particle located at its base. This abated selectivity for the S-rich sharpened tip may be elucidated by the fact that the Au monomer concentrations far exceed the threshold for nucleation at both tips of the nanorod. As shown in Figure 3(b), tetrapods with cone-like arms featured a dominant arm bearing a large Au tip. Deposition of Au at the tips of the other arms, as well as their sides, was scarcely perceptible at the magnification afforded by low resolution TEM. Tetrapods with wider conelike arms also displayed exclusive Au growth at a particular vertex, as evident in Figure 3c. In stark contrast, nearly uniformly spaced small Au particles were seen throughout the surface of each arm for tetrapods with cylinderlike arms as illustrated in Figure 3d, consistent with previous observations of Au deposition on hexagonal pencil-like CdS nanorods.[22] The remarkably enhanced selectivity for tip growth in the conelike versus cylinderlike CdS structures and the intriguing dominance of one arm for tip growth among four approximately symmetric tetrapod arms with S-rich tips cannot be explained by surface defect mediated growth alone, which asserts that unpassivated surfaces and areas of structural defects constitute the most chemically reactive sites and are therefore most likely to accommodate nucleation and growth of another material.[8b,23] Such a deposition mechanism would contradict the unusually high propensity for tip growth in the conelike structures given their likely higher density of unpassivated surface atoms at the side facets in comparison to those of cylinderlike structures. Moreover, ligand-exchange control experiments ruled out the effects of different capping groups on the observed deposition processes (see the Supporting Information for details, Figure S7).

This apparent conundrum may be better resolved by considering the electrochemical Ostwald ripening process previously reported in dumbbell-like Au-CdSe nanorods as mentioned earlier, where a decrease in the size of the Au at a particular tip results in an increase in Au particle size at the other tip.[10] It is interesting to note that in the case of Au-decorated CdS nanorods,[23] continued ripening effects over a period of days eventually resulted in a match-stick like configuration with a large dominant Au tip. Given our reaction conditions (ambient temperature, short growth times), there are two sets of experimental observations which have led us to conclude that the unique Au-semiconductor morphologies on our cone-like structures may be attributed to an enhanced electrochemical Ostwald ripening process. First, aliquots taken at early reaction times revealed the presence of Au particles of comparable sizes at the tips of all the arms of the tetrapods. After 40 min, an eventual depletion in the free monomers in solution resulted in the favored growth of one of the tips while the remaining tips were diminished in size as illustrated by a and b in Figure 4. Second, for tetrapods with conelike arms exposed to very high concentrations of Au precursor (such that growth of small Au clusters may be seen across the arms) at an elevated temperature of 90 °C for 1.5 h, comparison with the control experiment done at room temperature showed a dramatic decrease in the number of Au clusters at the sides of the arms, as evident in panels c and d in Figure 4. This finding is clearly in contradistinction with a surface defect based growth only model where the increased detachment rate of surface ligands at higher temperatures would result in the growth of more Au particles.[8b] On the other hand, higher reaction temperatures are expected to amplify Ostwald ripening

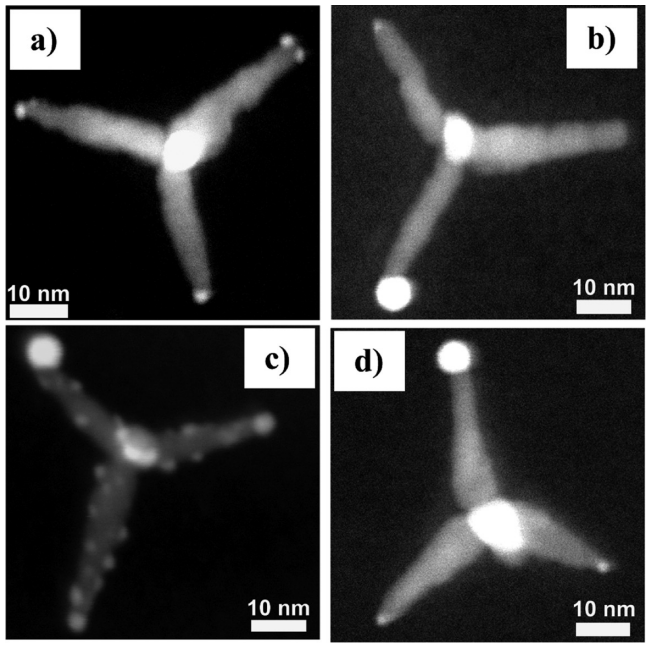

Figure 4. HAADF-STEM images of representative tetrapods with cone-like arms exposed to a fixed Au precursor concentration and allowed to react at room temperature for (a) 5 min and (b) 40 min; and at a much higher Au precursor concentration for 1.5 h at (c) room temperature and (d) 90 °C, respectively.

processes and yield less Au particles at the sides of the cone-like arms, in agreement with our HAADF-STEM data. In the case of CdSe tetrapods where electrochemical Ostwald ripening of the Au particles at the tips of the different arms toward a single dominant arm was reported not to occur, it was suggested that the presence of a barrier prevented electron transfer between the rod arms that was necessary for the electrochemical Ostwald ripening process to take place. The origins of the barrier were hypothesized to stem from structural defects at the interface between the zinc-blende and wurtzite lattice of the CdSe core and arms respectively.[10] In the case of our cone-like tetrapods, it is reasonable to expect that electron hopping across surface states can take place throughout wurtzite CdS, which constitutes both the arm and shell material around the zb-CdSe core.

To demonstrate an exemplary utility of the unique propensity for Au to be deposited onto a single tip of a near-symmetric 4-arm tetrapod and circumventing an expected Poissonian distribution of Au tip growth, we attempted to fabricate hierarchically complex tetrapod structures with one tip specifically functionalized with a single Au particle while the other tips possess Ag_2S particles. This was achieved by depositing Au and Ag precursors in a sequential manner, which was previously used to synthesize Janus-like dumbbell nanorod structures.[9] Unlike Au, the Ag precursors do not nucleate and grow on the CdS surface but spontaneously forms Ag_2S particles via cationic exchange with Cd^{2+}.[24] By first directing Au growth at the tip of one of the tetrapod arms, facets at the vertex of that arm are rendered inaccessible by Ag^+ and cationic exchange occurs at the tips of the other arms instead. An illustration of this strategy is given in Figure 5a. The as-synthesized structures are depicted in Figure 5b, which is a representative HAADF-STEM image showcasing the potentially high degree of synthetic control over the fabrication of asymmetrically tipped tetrapod nanostructures. A total of 10

dx.doi.org/10.1021/cm300161m | Chem. Mater. 2012, 24, 2040−2046

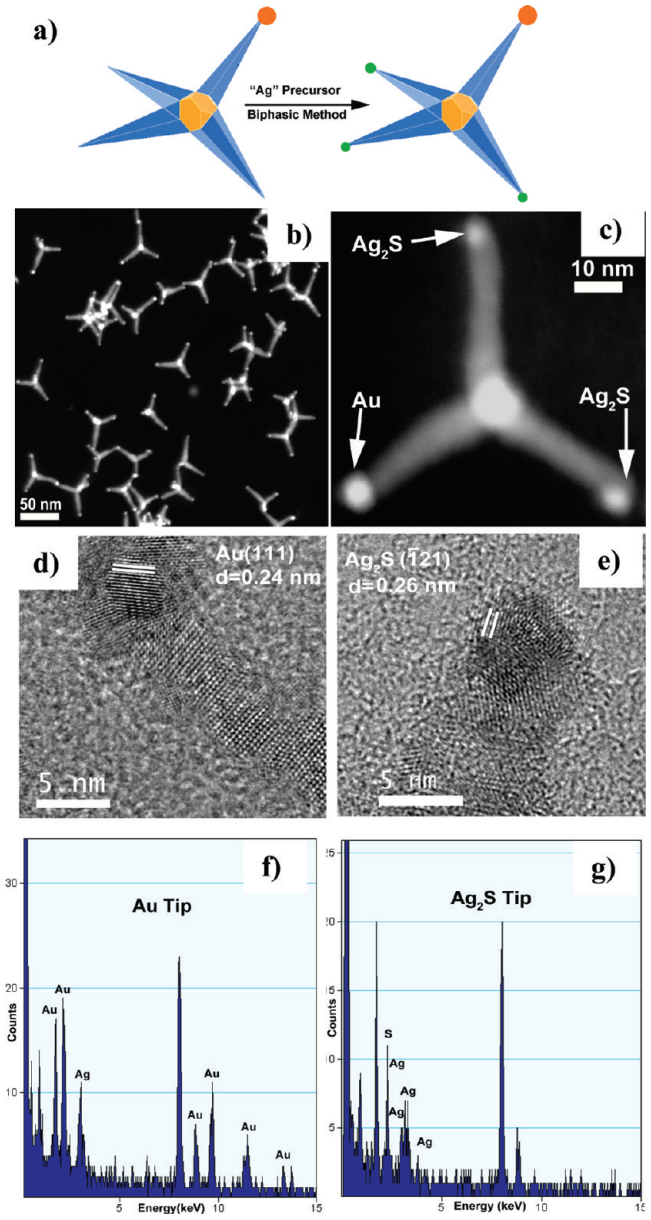

Figure 5. (a) Reaction schematic to obtain hierarchically complex CdSe-seeded CdS tetrapods with Au at precisely one tip and Ag_2S at the other three. (b) Representative HAADF-STEM image of tetrapods with conelike arms fabricated according to the strategy shown in a. (c) Magnified view of one of the tetrapods in b, with the different tips labeled. (d, e) HRTEM images of the different tetrapod arm tips showing the visible lattice fringes of the Ag_2S ($\bar{1}21$) and Au (111) planes with measured *d*-spacings of 0.26 and 0.24 nm, respectively. Further confirmation of the (f) Au and (g) Ag_2S tip elemental composition by EDX, respectively.

randomly chosen tetrapods were analyzed via HAADF-STEM and EDX, as may be seen from Figure 5b–f, which collectively exemplify the absence of nanoparticles at the side facets of the arms, and tips with materials composition in accordance with our hypothesized structure. Although the deposition of Ag on the Au particle was occasionally observed, it should be pointed out that the protocols for the synthesis of these structures remains largely unoptimized, and incremental improvements such as minimizing the deposition of Ag on the Au particle may be effected via a more judicious choice of Ag precursor concentrations. Nevertheless, the monodispersity of the complex tetrapod configurations obtained attests to our approach to asymmetric nanoparticle growth at the tips of branched semiconductor nanostructures in a relatively controlled manner.

CONCLUSIONS

In summary, we have described the synthesis and characterization of cone-like nanorods and tetrapods via the use of a combination of carboxylic and alkyl phosphonic ligands. The cone-like nanorods and tetrapods were compared with their more conventional cylinderlike counterparts in terms of their topological selectivity of Au deposition. A remarkably higher propensity for tip growth was found in the case of the conelike structures, with an unexpected single-tip growth in the case of tetrapods. This was ascribed to a dramatically enhanced intraparticle electrochemical Ostwald ripening process in which small Au clusters at the side facets of the semiconductor structure were rapidly dissolved and redeposited onto the large Au particles at the tips. The resulting one-tipped Au-semiconductor tetrapods were subsequently exploited to produce uniform hierarchically complex tetrapod structures with Au on one tip and Ag_2S at the other three, thus exemplifying a strategy for circumventing a statistical distribution of tips with different materials composition. We envision that an appropriate sequential deposition of suitable metals may lead to uniform tetrapod structures with metal tips of different composition, thus presenting intriguing scenarios for conductivity studies in branched semiconductor structures at the single nanoparticle level.

ASSOCIATED CONTENT

Supporting Information

XRD, UV–vis, HRTEM, and NMR characterization data. This material is available free of charge via the Internet at http://pubs.acs.org.

AUTHOR INFORMATION

Corresponding Author

*E-mail: chmchany@nus.edu.sg.

Author Contributions

All authors have given approval to the final version of the manuscript.

Notes

The authors declare no competing financial interest.

ACKNOWLEDGMENTS

We would like to thank Tanay Pramanik and Mingyu Hu for their assistance in the NMR measurements. This work was supported by National University of Singapore (Start-up grant WBS R143-000-367-133), DSTA (grant WBS R143-000-423-422), and TSRP-A*STAR (grant WBS R143-000-435-305).

REFERENCES

(1) Sheldon, M. T.; Trudeau, P. E.; Mokari, T.; Wang, L. W.; Alivisatos, A. P. *Nano Lett.* **2009**, *9*, 3676–3682.

(2) (a) Costi, R.; Saunders, A. E.; Salant, A.; Banin, U. *Nano Lett.* **2008**, *8*, 637–641. (b) Amirav, L.; Alivisatos, A. P. *J. Phys. Chem. Lett.* **2010**, *1*, 1051–1054. (c) Berr, M.; Vaneski, A.; Susha, A. S.; Rodríguez-Fernández, J.; Döblinger, M.; Jäckel, F.; Rogach, A. L.; Feldmann, J. *Appl. Phys. Lett.* **2010**, *97*, 093108(1–3). (d) Acharya, K. P.; Khnayzer, R. S.; O'Connor, T.; Diederich, G.; Kirsanova, M.; Klinkova, A.; Roth, D.; Kinder, E.; Imboden, M.; Zamkov, M. *Nano Lett.* **2011**, *11*, 2919–2926.

(3) Li, X.; Lian, J.; Lin, M.; Chang, Y. *J. Am. Chem. Soc.* **2011**, *133*, 672−675.
(4) Figuerola, A.; Franchini, I. R.; Fiore, A.; Mastria, R.; Falqui, A.; Bertoni, G.; Bals, S.; Tendeloo, G. V.; Kudera, S.; Cingolani, R.; Manna, L. *Adv. Mater.* **2009**, *21*, 550−554.
(5) Zhao, N.; Vickery, J.; Guerin, G.; Park, J. I.; Winnik, M. A.; Kumacheva, E. *Angew. Chem., Int. Ed.* **2011**, *50*, 4606−4610.
(6) (a) Salant, A.; Amitay-Sadovsky, E.; Banin, U. *J. Am. Chem. Soc.* **2006**, *128*, 10006−10007. (b) Zhao, N.; Liu, K.; Greener, J.; Nie, Z.; Kumacheva, E. *Nano Lett.* **2009**, *9*, 3077−3081.
(7) (a) Mokari, T.; Rothenberg, E.; Popov, I.; Costi, R.; Banin, U. *Science* **2004**, *304*, 1787−1790. (b) Menagen, G.; Mocatta, D.; Salant, A.; Popov, I.; Dorfs, D.; Banin, U. *Chem. Mater.* **2008**, *20*, 6900−6902. (c) Khalavka, Y.; Sönnichsen, C *Adv. Mater.* **2008**, *20*, 588−591.
(8) (a) Carbone, L.; Jakab, A.; Khalavka, Y.; Sönnichsen, C. *Nano Lett.* **2009**, *9*, 3710−3714. (b) Menagen, G.; Macdonald, J. E.; Shemesh, Y.; Popov, I.; Banin, U. *J. Am. Chem. Soc.* **2009**, *131*, 17406−17411.
(9) Chakrabortty, S.; Yang, J. A.; Tan, Y. M.; Mishra, N.; Chan, Y. *Angew. Chem., Int. Ed.* **2010**, *49*, 2888−2892.
(10) Mokari, T.; Sztrum, C. G.; Salant, A.; Rabani, E.; Banin, U. *Nat. Mater.* **2005**, *4*, 855−863.
(11) Yang, Y. A.; Wu, H.; Williams, K. R.; Cao, Y. C. *Angew. Chem., Int. Ed.* **2005**, *44*, 6712−6715.
(12) Snee, P. T.; Chan, Y.; Nocera, D. G.; Bawendi, M. G. *Adv. Mater.* **2005**, *17*, 1131−1136.
(13) Leatherdale, C. A.; Woo, W. K.; Mikulec, F. V.; Bawendi, M. G. *J. Phys. Chem. B* **2002**, *106*, 7619−7622.
(14) Carbone, L.; Nobile, C.; De Giorgi, M.; Della Sala, F.; Morello, G.; Pompa, P.; Hytch,, M.; Snoeck, E.; ,Fiore, A.; Franchini, I. R.; et al. *Nano Lett.* **2007**, *7*, 2942−2950.
(15) Talapin, D. V.; Nelson, J. H.; Shevchenko, E. V.; Aloni, S.; Sadtler, B.; Alivisatos, A. P. *Nano Lett.* **2007**, *7*, 2951−2959.
(16) Yang, J.; Levina, L.; Sargent, E. H.; Kelley, S. O. *J. Mater. Chem.* **2006**, *16*, 4025−4028.
(17) Fiore, A.; Mastria, R.; Lupo, M. G.; Lanzani, G.; Giannini, C.; Carlino, E.; Morello, G.; Giorgi, M. D.; Li, Y.; Cingolani, R.; Manna, L. *J. Am. Chem. Soc.* **2009**, *131*, 2274−2282.
(18) Manna, L.; Scher, E. C.; Alivisatos, A. P. *J. Cluster Sci.* **2002**, *13*, 521−532.
(19) Mahler, B.; Lequeux, N.; Dubertret, B. *J. Am. Chem. Soc.* **2010**, *132*, 953−959.
(20) (a) Huang, X.; Zhao, Z.; Fan, J.; Tan, Y.; Zheng, N. *J. Am. Chem. Soc.* **2011**, *133*, 4718−4721. (b) Katz-Boon, H.; Rossouw, C. J.; Weyland, M.; Funston, A. M.; Mulvaney, P.; Etheridge, J. *Nano Lett.* **2011**, *11*, 273−278.
(21) Baski, A. A.; Whitman, L. J. *Phys. Rev. Lett.* **1995**, *74*, 956−959.
(22) Saruyama, M.; Kanehara, M.; Teranishi, T. *J. Am. Chem. Soc.* **2010**, *132*, 3280−3282.
(23) Saunders, A. E.; Popov, I.; Banin, U. *J. Phys. Chem. B* **2006**, *110*, 25421−25429.
(24) Robinson, R. D.; Sadtler, B.; Demchenko, D. O.; Erdonmez, C. K.; Wang, L. W.; Alivisatos, A. P. *Science* **2007**, *317*, 355−358.